

Oscillatory Swirling Flows in a Cylindrical Enclosure with Co-/Counter-Rotating end Disks Submitted to a Vertical Temperature Gradient

Brahim Mahfoud¹ and Rachid Bessaih^{1,2}

Abstract: Oscillatory swirling flows in a cylindrical enclosure, having aspect ratio (height/radius) $\gamma=2$, filled with a liquid metal, and submitted to a destabilizing vertical temperature gradient (system heated from below) is investigated by means of direct numerical solution of the governing (continuity, radial and axial momentum, swirl and energy) equations. The bottom and top disks are assumed to rotate at equal (co-rotating) and opposite (counter-rotating) angular velocities. The critical Reynolds number, Re_{cr} and the critical frequency of oscillations, F_{cr} are calculated as a function of the Richardson number, Ri , ranging between 0 and 4. Stability diagrams are presented, reflecting the results of the numerical investigation, which put in evidence the dependence of Re_{cr} and F_{cr} on Ri . In particular, it is found that the increase of Ri causes the decrease of Re_{cr} . The study is accompanied by a grid refinement and validation analysis based on comparison with other relevant results in the literature.

Keywords: Oscillatory, Co-/counter-rotating, Swirling flows, Cylinder.

Nomenclature

F	dimensionless frequency
g	acceleration due to gravity m/s^2
Gr	Grashof number
H	height of the cylinder m
N_{ech}	number of samples
P	dimensionless pressure
Pr	Prandtl number
R	radius of the cylinder m

¹ LEAP Laboratory, Faculty of Engineering, Dept. of Mechanical Engineering, University of Mentouri-Constantine, Algeria.

² Corresponding author: Bessaih.rachid@gmail.com, Phone/Fax: +213 31 81 88 63

r	dimensionless radial coordinate
z	dimensionless axial coordinate
Re	Reynolds number
Ri	Richardson number
T	temperature K
u	dimensionless radial velocity component
v	dimensionless axial velocity component
w	dimensionless azimuthal velocity component

Greek symbols

α	thermal diffusivity of the fluid m^2/s
β	thermal expansion coefficient K^{-1}
γ	aspect ratio
Θ	dimensionless temperature
ν	kinematic viscosity of the fluid m^2/s
ρ	density of the fluid kg/m^3
Ω	angular velocity rad/s
τ	dimensionless time
ψ	dimensionless stream function

Indices

a,b,c,d,e,f,g,h	corresponding to various times
cr	critical value
c	cold
h	hot
r, z, θ	radial, axial and azimuthal directions, respectively

1 Introduction

Flows between two rotating disks were the subject of many studies. These flows model natural situations in astrophysics (Hart and Kittelman, 1996) and meteorology (Knobloch, 1998), but also the devices such as: rotating machinery (Hirano et al., 2005), rotational viscometers (Weltmann and Kuhns, 1952), computer storage devices and material processing units (Jaluria, 2001), centrifugal machinery (Yu et al., 2000), and pumping of liquid metals at high melting point (Barnes, 1955).

Several theoretical, experimental and numerical studies were undertaken on the stability of rotating flows. Following von Kármán's similarity solution of the Navier-Stokes equations for steady flow near a rotating disk, Batchelor (1951) analyzed the general nature of the flow and predicted that in almost all cases, the main body of fluid is rotating. For the case of counter-rotating disks, he pointed out that the main body of the fluid would be in two parts with different rotation rates. Shortly afterwards, Stewartson (1953) showed that the fluid in the core would not rotate when the top and bottom disks counter rotate exactly. For the flows in the cylindrical enclosure with the rotating top disk and co-/counter-rotating sidewall and bottom disk, velocity distribution similar to both Batchelor and Stewartson types was observed depending on the value of parameters (Dijkstra and Heijst, 1983). Transition from steady to unsteady oscillatory flows was investigated by Lopez (1998). Gelfgat et al. (1996a) analyzed the linear stability of the steady state solutions with respect to axisymmetric disturbances for homogeneous fluid confined in cylinders with co-/counter-rotating top and bottom disks. The stability of steady flows in the cylinder with rotating end disks was studied by Gelfgat et al. (1996b) for aspect ratios $1 < \gamma < 3.5$. It was shown that for $\gamma < 3$, the oscillatory instability sets in as a result of an axisymmetric Hopf bifurcation.

In many practical applications, heat transfer is associated with the rotating fluid flows. Considerable amount of previous investigations have directed toward the convection and instabilities in connection with the crystal growth processing units, where thermally unstable boundary conditions are imposed (Jaluria, 2001). It appears that a relatively small amount of studies have been done on the laminar rotating flow confined in containers under stable temperature difference. Kim and Hyun (1997) studied the swirling flow between finite disks under stabilizing temperature difference, for sealed cylindrical container when one of the end disks is rotating. Valentine and Jahnke (1994) examined the flow field inside a cylindrical enclosure induced by the rotation of the top and bottom end walls with a fixed sidewall; a stable oscillatory solution was found for a Reynolds number $Re=3103$ and an aspect ratio $\gamma=1.5$. A numerical study of the periodic flow for $\gamma=2.5$ was conducted by Lopez and Perry (1992), who showed the existence of oscillatory modes. Stevens et al. (1999) performed a combined experimental and numerical investigation to highlight multiple oscillatory states, which exist in the flow of a fluid confined in a cylindrical cavity of aspect ratio $\gamma=2.5$, with a rotating end wall. They identified three oscillating states: two of them being periodic and the third being quasi-periodic with a modulation frequency much smaller than the base frequency. Xinjun (2003) reported numerical simulations of the Navier–Stokes equations for the axisymmetric recirculating zones during spin-up and spin-down for confined rotating fluid flows.

Iwatsu (2004) numerically examined the heat transfer characteristics of rotating viscous, incompressible and axisymmetric fluid flow generated by the constant rotation of the top disk in a cylindrical enclosure of aspect ratio $\gamma=1$. He presented steady state solutions obtained for the ranges of controlling parameters: the Reynolds number $10^2 \leq Re \leq 3 \times 10^3$, the Richardson number, $0 \leq Ri \leq 1.0$, and the Prandtl number $Pr=1$. Omi and Iwatsu (2005) investigated numerically swirling flows of a Boussinesq fluid confined in a cylindrical container with co-/counter-rotating end disks. Cui (2008) discussed the flow driven by the counter rotating end wall or sidewall in a fluid-filled cylinder. Several variants of the subject were investigated according to the way in which rotation was applied to the system. Such instabilities and bifurcation are still attracting much attention nowadays, e.g. Nore et al. (2003 and 2004). Gelfgat et al. (2001) performed a linear stability analysis of the steady axisymmetric base flow in the range $\gamma \in [1, 3.5]$ and found that for $1.63 \leq \gamma \leq 2.76$, the first bifurcation is to an axisymmetric and oscillatory state. Outside this range, the instability is not axisymmetric and azimuthal wave numbers $m=2, 3$ or 4 dominate. Recent numerical articles include axisymmetric simulations (Bordja et al., 2010).

The present work investigates numerically the determination of hydrodynamic and thermal instabilities, which are created in a cylindrical container with co-/counter-rotating end disks. Our numerical simulations are presented for various values of the Richardson number ($Ri = 0, 0.5, 1, 2$, and 4). Stability diagrams ($Re_{cr}-Ri$) and ($F_{cr}-Ri$) are plotted and discussed in this paper.

2 Geometry and mathematical model

We consider a cylindrical enclosure (Fig. 1) of radius R and height H , having an aspect ratio $\gamma=H/R=2$. The cylinder contains a liquid metal characterized by a small Prandtl number ($Pr=0.015$). The bottom disk is rotating with a constant angular velocity Ω , and is maintained at a hot temperature T_h , while the top disk is in co-/counter-rotating and maintained at the temperature $T_c (T_c < T_h)$. The sidewall of the cylinder is adiabatic. We refer to the boundary conditions as "co-rotating" when the top and the bottom disks rotate with the same angular velocity, and "counter-rotating" when end disks rotate in opposed direction with the same angular velocity Ω .

Adopting the same assumptions, as in the work of Bessaih et al.(2003), employing the Boussinesq approximation, and introducing the scales $1/\Omega$ for time, R for lengths, ΩR for velocities, $\rho(\Omega R)^2$ for pressure, and $T_h - T_c$ for temperature; the dimensionless form of the governing equations can be written as follow:

Continuity equation:

$$\frac{1}{r} \frac{\partial(ru)}{\partial r} + \frac{\partial v}{\partial z} = 0 \quad (1)$$

r-Momentum equation:

$$\frac{\partial u}{\partial \tau} + u \frac{\partial u}{\partial r} + v \frac{\partial u}{\partial z} - \frac{w^2}{r} = -\frac{\partial P}{\partial r} + \frac{1}{Re} \left(\frac{1}{r} \frac{\partial}{\partial r} \left(r \frac{\partial u}{\partial r} \right) + \frac{\partial^2 u}{\partial z^2} - \frac{u}{r^2} \right) \quad (2)$$

z-Momentum equation:

$$\frac{\partial v}{\partial \tau} + u \frac{\partial v}{\partial r} + v \frac{\partial v}{\partial z} = -\frac{\partial P}{\partial z} + \frac{1}{Re} \left(\frac{1}{r} \frac{\partial}{\partial r} \left(r \frac{\partial v}{\partial r} \right) + \frac{\partial^2 v}{\partial z^2} \right) + Ri \cdot \Theta \quad (3)$$

Swirl equation:

$$\frac{\partial w}{\partial \tau} + u \frac{\partial w}{\partial r} + v \frac{\partial w}{\partial z} + \frac{uw}{r} = \frac{1}{Re} \left(\frac{1}{r} \frac{\partial}{\partial r} \left(r \frac{\partial w}{\partial r} \right) + \frac{\partial^2 w}{\partial z^2} - \frac{w}{r^2} \right) \quad (4)$$

Energy equation:

$$\frac{\partial \Theta}{\partial \tau} + u \frac{\partial \Theta}{\partial r} + v \frac{\partial \Theta}{\partial z} = \frac{1}{Re \cdot Pr} \left(\frac{1}{r} \frac{\partial}{\partial r} \left(r \frac{\partial \Theta}{\partial r} \right) + \left(\frac{\partial^2 \Theta}{\partial z^2} \right) \right) \quad (5)$$

where u , v and w are the dimensionless radial, axial and azimuthal velocity, respectively, P is the dimensionless pressure and $\Theta = (T - T_c) / (T_h - T_c)$ is the dimensionless temperature. In Eqs (2)–(5), $Re = \Omega R^2 / \nu$ is the Reynolds number, $Ri = Gr / Re^2$ is the Richardson number, which expresses the ratio of the buoyancy forces to the inertia forces induced by the disk rotation, and $Pr = \nu / \alpha$ is the Prandtl number. The Grashof number is defined as $Gr = g \beta (T_h - T_c) R^3 / \nu^2$, where g and β are the gravity acceleration and the thermal expansion coefficient, respectively.

Eqs. (1)–(5) are subjected to the following initial and boundary conditions:

The initial conditions, at $\tau=0$, are :

$$u = 0, \quad v = 0, \quad w = 0, \quad \Theta = 0, \quad (0 < r < 1, \quad 0 < z < 2) \quad (6a)$$

The boundary conditions of the dimensionless quantities (u , v , w , and Θ), for $\tau > 0$ are:

at $r=0$ and $0 \leq z \leq 2$:

$$u = 0, \quad \frac{\partial v}{\partial r} = 0, \quad w = 0, \quad \frac{\partial \Theta}{\partial r} = 0 \quad (6b)$$

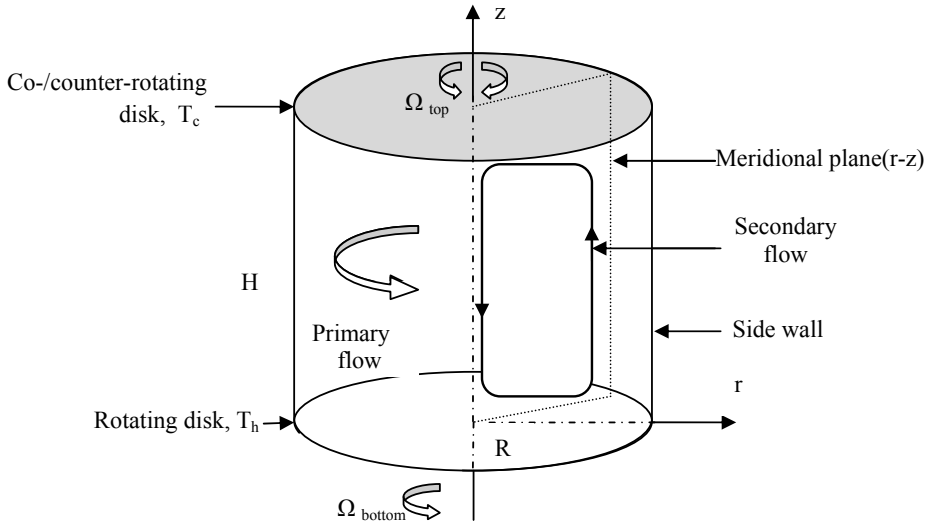


Figure 1: Geometry of the physical problem.

at $r=1$ and $0 \leq z \leq 2$:

$$u = 0, \quad v = 0, \quad w = 0, \quad \frac{\partial \Theta}{\partial r} = 0 \quad (6c)$$

at $z=0$ and $0 \leq r \leq 1$:

$$u = 0, \quad v = 0, \quad w = r, \quad \Theta = 1 \quad (6d)$$

Co-rotating case:

at $z=2$ and $0 \leq r \leq 1$:

$$u = 0, \quad v = 0, \quad w = r, \quad \Theta = 0 \quad (6e)$$

Counter-rotating case:

at $z=2$ and $0 \leq r \leq 1$:

$$u = 0, \quad v = 0, \quad w = -r, \quad \Theta = 0 \quad (6f)$$

3 Numerical method

The governing equations were solved using a finite volume method, as described by Patankar (1980). Scalar quantities (P , w and Θ) are stored at the center of these

volumes, whereas the vectorial quantities (u and v) are stored on the faces of each volume. For the discretisation of spatial terms, a second-order central difference scheme is used for the diffusion and convection parts of Eqs. (2)– (5), and the SIMPLER algorithm (Patankar, 1980) is used to solve the coupling between velocity and pressure. Prior to the execution of parametric computation, grid independency of the numerical solution is assessed for representative parameter values by changing the number of grid points. The number of grid points used in these resolution tests is shown in Table 2. The results are listed in terms of the maximum and minimum values of the stream function ψ (defined as : $u = \frac{1}{r} \frac{\partial \psi}{\partial z}$).

According to Table 2, difference in the minimum value between coarse and medium grids is less than 0.7%, and that between the medium and fine grids is less than 0.6%. The influence of structured mesh size was checked at a representative set of the radial velocity u plotted at $r = 0.89$ and the axial velocity v plotted at $z=1.02$, for $Re=600$ and $Ri=1$ (Fig.2). The result of this grid independency check was that the thin curve deviation between the medium grid system with 80×160 nodes and the fine grid system with 90×180 nodes. The grid spacing in r and z directions are not regular. They were chosen according to geometric progressions of ratio 1.05, which permitted grid refinement near the walls. The grid used has 80×160 nodes and was chosen after performing grid independency tests. This grid is considered to show the best compromise between computational time and precision. Calculations were carried out on a PC with Core2 Duo 1.6 GHz CPU. Thus, the average computing time for a typical case was approximately three days.

4 Results and discussion

4.1 Validation of the code

The accuracy of our numerical code is checked by comparing the present results with the numerical investigations found in the literature. Our results are first compared with the numerical work of Gelfgat et al. (1996), which have used the Galerkin spectral method with 30×30 basis functions. Lopez (1995) and Iwatsu (2005) have used stretched grid with second order finite difference method. Brøns et al. (2001) have used uniform grid with combined second/fourth order finite difference method (Table 3). The maximum deviation in the value of the critical Reynolds number Re_{cr} for the steady-to unsteady transition between the present and previous numerical simulations is 6%. The second comparison with the numerical work of Gelfgat et al. (1996) is shown in Table 4. The authors present a numerical investigation of steady states, onset of oscillatory instability, and slightly supercritical oscillatory states of an axisymmetric swirling flow of a Newtonian incompressible fluid in a cylinder, with independently rotating top and bottom.

Table 1: Dimensionless coordinates of the monitoring points S1, S2, S3, S4, S5, S6, S7, S8, and S9.

Monitoring points	S1	S2	S3	S4	S5	S6	S7	S8	S9
r	0.201	0.493	0.802	0.201	0.493	0.802	0.201	0.493	0.802
z	0.413	0.413	0.413	0.975	0.975	0.975	1.779	1.779	1.779

Table 2: Influence of the number of grid points on the maximum and minimum values of the stream function ψ , for several values of Re in the vicinity of the critical Reynolds number Re_{cr} for steady-to-unsteady transition.

unsteady transition.

$n_r \times n_z$	Re	Coarse 70×140 nodes		Medium 80×160 nodes		Fine 90×180 nodes		
		min	max	min	max	min	max	
Co-rotating								
0	2640	-0.00738	0.00737	-0.00737	0.00739	-0.00736	0.00737	
0.5	1472	-0.03965	0.03964	-0.03963	0.03964	-0.03968	0.03967	
1	925	-0.04369	0.04368	-0.04338	0.04345	-0.04355	0.04395	
2	640	-0.04816	0.04813	-0.04818	0.04816	-0.04815	0.04816	
4	440	-0.05633	0.05631	-0.05635	0.05634	-0.05632	0.05633	
Counter-rotating								
0	2280	-0.00727	0.00727	-0.00728	0.00728	-0.00726	0.00726	
0.5	1270	-0.00689	0.00690	-0.00688	0.00695	-0.00689	0.00693	
1	940	-0.06154	0.06153	-0.06156	0.06156	-0.06159	0.06158	
2	640	-0.07475	0.07470	-0.07471	0.07472	-0.07476	0.07476	
4	440	-0.07513	0.07513	-0.07515	0.07514	-0.07518	0.07516	

The third comparison is made with numerical the simulations obtained by Iwatsu (2005), see Fig.3. It is clear that the computed values are in excellent agreement with predictions.

In unsteady state, we compare our results (Fig.4) with the numerical study of Gelfgat et al.(1996). They present the instantaneous streamlines of the meridional flow plotted for equal time intervals $0.1T$, covering the complete period $T=13.01$, $\gamma=1.5$ (co-rotating case) and $Re=3845$ (for detail, see Gelfgat et al., 1996).

4.2 Oscillatory flow

In this section, we present the results about the transition from steady to oscillatory flow for both cases of co-and counter-rotating end disks (together with a critical discussion of the influence exerted on the system by other parameters). Both the critical Reynolds numbers, Re_{cr} and the critical frequency of oscillation, F_{cr} are determined.

It is a well-known fact that the typical sequence of evolution of a dynamic system towards chaos for increasing values of the control parameter consists of the following stages: transition to an oscillatory or periodic state; a quasi-periodic regime, and finally chaos (or turbulence). Here the critical Reynolds number corresponds to the threshold of the oscillating regime.

We detected the physical instability, performing a series of numerical calculations by increasing the Reynolds number in predetermined intervals, for each Richardson number ($Ri=0, 0.5, 1, 2, 4$). As an example, the solution just before the onset of oscillations for $Ri=1$ is shown in Fig 5 ($Re=900$ and $Re=926$). The oscillatory instability for a given dimensionless time-step $\Delta\tau$ (Fig.5) and $Re_{cr}=928$ was found to be of a numerical nature (not physical); for this reason we recomputed the solution for the same flow parameters, but with a time-step $\Delta\tau/2$. In general, to detect instabilities of a physical nature, we introduced a criterion based on “observation” points (S1 to S9, their positions being defined in Table 1), to monitor simultaneously the temporal evolutions of dimensionless velocity components in the radial, azimuthal and axial directions, the dimensionless temperature Θ , and the values of stream function ψ in the meridional plane (r - z) until the system reaches an asymptotic state with oscillation amplitude no longer dependent on time.

The critical values of the Reynolds number Re_{cr} for each value of the Richardson number ($Ri=0, 0.5, 1, 2$ and 4) are summarized in Table 5, and two related dependence diagrams (Re_{cr} - Ri) and (F_{cr} - Ri) are plotted in Figs 12a-b. At same time, we consider a comparison between co-rotation and counter-rotating end disks.

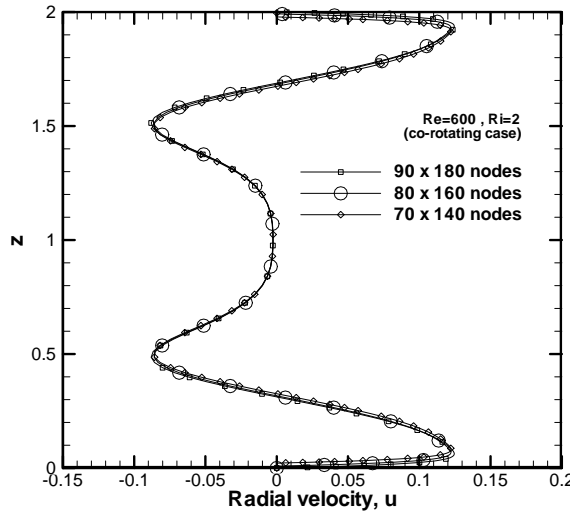
The primary flow is represented by the azimuthal velocity w , while the secondary flow is characterized here with u, v and ψ .

Table 3: Comparison with previous numerical studies, for the influence of the grid resolution on the critical Reynolds number Re_{cr} for steady-to-unsteady transition (where $n_r \times n_z$ denotes the number of discrete elements). Gelfgat et al. (1996) used Galerkin spectral method with 30×30 basis functions. Lopez (1995) and Iwatsu (2005) used stretched grid with second order finite difference method. Brøns et al. (2001) used uniform grid with combined second/fourth order finite difference method.

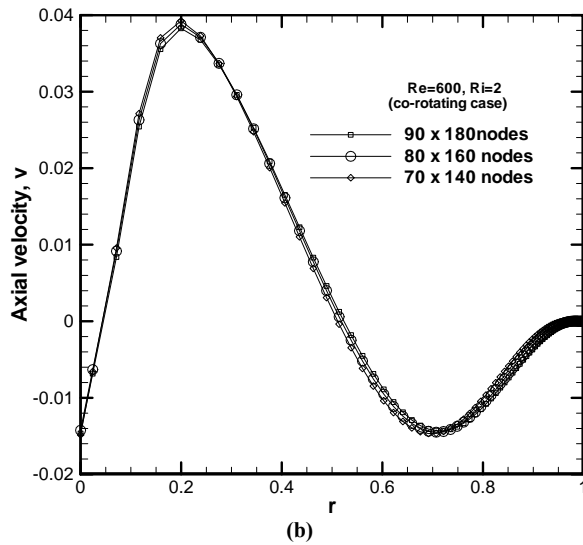
	Gelfgat <i>et al.</i> (1996)	Lopez (1995)	Brøns <i>et al.</i> (2001)	Iwatsu (2005)	Present study
$n_r \times n_z$	30×30	101×151	$100/\gamma \times 100$ $100 \times 100/\gamma$	161×161 161×321	80×160
$\gamma=0.5$	6745		6246	4248	
$\gamma=0.75$	3846		3714	3812	
$\gamma=1.0$	2567		2564	2384	2406
$\gamma=1.5$	2663	2640	2636	2674	2750
$\gamma=2.0$			2921	2555	2605
$\gamma=2.5$			2725	2697	2715
$\gamma=3.0$			3046	2977	2995
$\gamma=3.5$			3316	3315	
$\gamma=4.0$			3659	3635	3640

Table 4: Comparison between our numerical results and the numerical simulations of Gelfgat et al. (1996)

$\gamma=1.5$	Gelfgat et al.(1996)							Present study $n_r \times n_z = 80 \times 160$
		30×30 Basis functions	32×32 Basis functions	34×34 Basis functions	36×36 Basis functions	38×38 Basis functions	40×40 Basis functions	
$\xi=1$ (co-rotating)	Re_{cr}	3846	3843	3843	3842	3843	3845	3830
	F_{cr}	0.4845	0.4842	0.4840	0.4840	0.4840	0.4840	0.4712
$\xi=1$ (counter-rotating)	Re_{cr}	1700	1669	1656	1649	1646	1644	1640
	F_{cr}	0.2887	0.2859	0.2848	0.2842	0.2839	0.2837	0.2801



(a)



(b)

Figure 2: Dimensionless axial velocity distribution: (a) along a vertical line at $r = 0.89$, (b) along a radial line at $z = 1.02$.

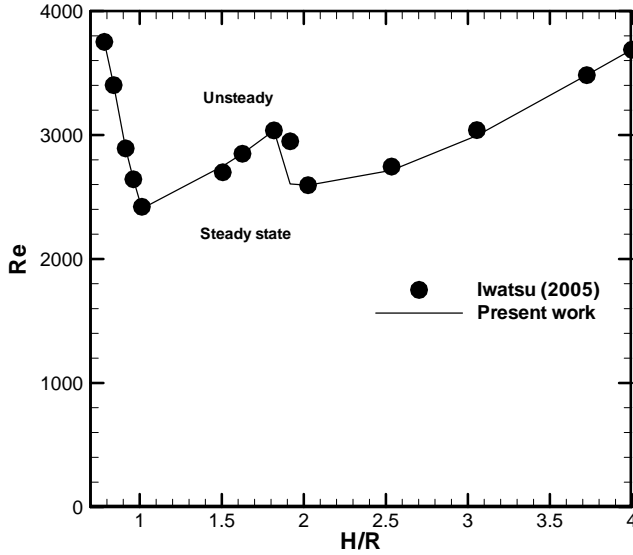


Figure 3: Comparison between our present results and the numerical simulations of Iwatsu (2005)

The periodic aspect of the axial velocity recorded at monitoring point S5 (Fig.5) indicates that oscillatory instabilities start, and that the flow undergoes a bifurcation. The origin of this instability can be ascribed to one of the two shear layers of this problem, namely the Ékman layer near the rotating disks or the so-called Stewartson layer along the vertical wall. By comparing the amplitude of oscillations, we can notice that the fluctuating component varies from a monitoring point to another, while the frequencies of oscillations (Fig.6a) are the same everywhere in the fluid, confirming the periodic character of the flow, as mentioned by Lopez and Perry (1992). The portraits phase (Fig.6b) is used to determine in a way intuitive and reliable the system behaviour in the phase space (this representation gives a limiting point for the steady state or a limit cycle in the oscillatory regime).

The temporal evolutions of dimensionless velocity components in the radial, azimuthal, and axial directions and temperature for $Re_{cr}=448$ and $Ri=4$ are shown in Fig.7a (co-rotating case) at monitoring point S2 (0.493, 0.413). In order to obtain the energy spectrum of oscillations, we have used the Fast Fourier Transform (FFT) of a number N_{ech} of samples of the time variations of various dimensionless parameters. The dimensionless predominant frequencies are considered as those playing the main role in the flow oscillation; there can exist several others frequencies which are multiples of the dominant one (Stevens et al., 2003). The previ-

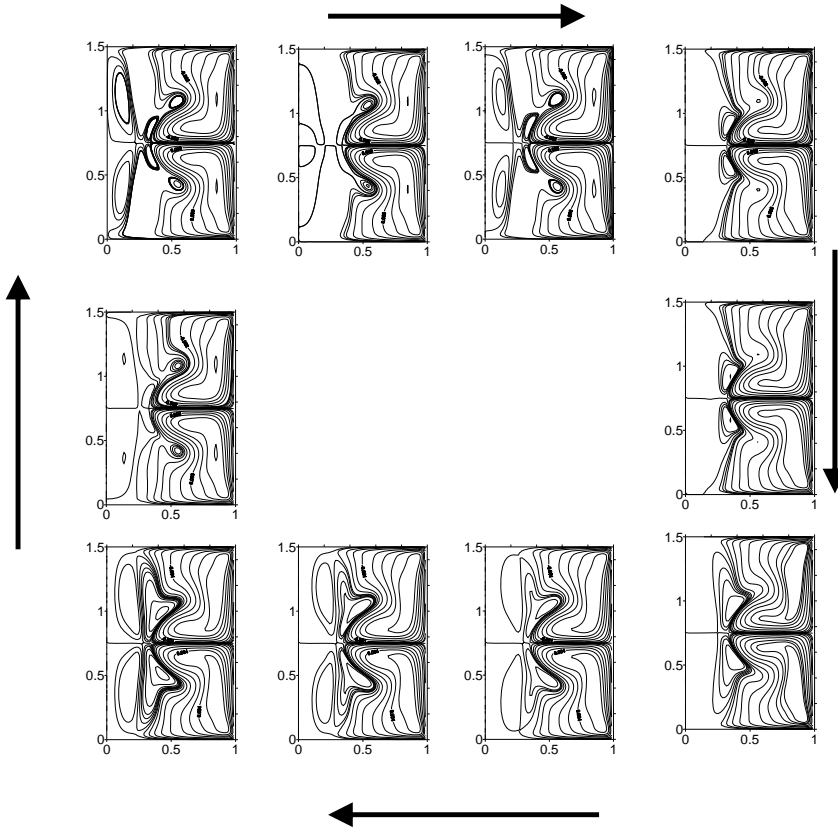


Figure 4: Comparison with the numerical results of Gelfgat et al. (1996) of instantaneous streamlines of the meridional flow plotted for equal time intervals $0.1T$, covering the complete period $T=13.01$. $\gamma=1.5$ and $Re=3845$ (co-rotating end disks case).

ous scenario (co-rotation) was found to be somewhat modified when dealing with counter-rotation end disks for which a new type of structure is formed.

Concerning the flow, the major concern is related to the precise determination of the critical Reynolds number which seems to be delicate, time consuming and may need a powerful computing able to calculate the temporal evolutions of this type of flow. The oscillatory aspect of the temporal evolutions of the flow parameters u , v , w , and Θ recorded at various points is shown in Fig.7b for $Re_{cr}=449$ and $Ri=4$ (counter-rotating case) at point S2. The remarks concerning the oscillatory behavior of the various parameters for the case of co-rotation are applicable to this

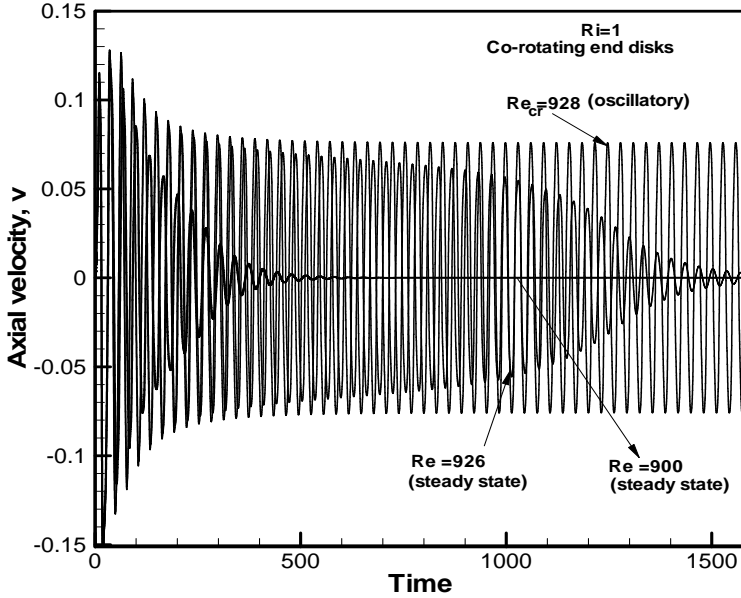
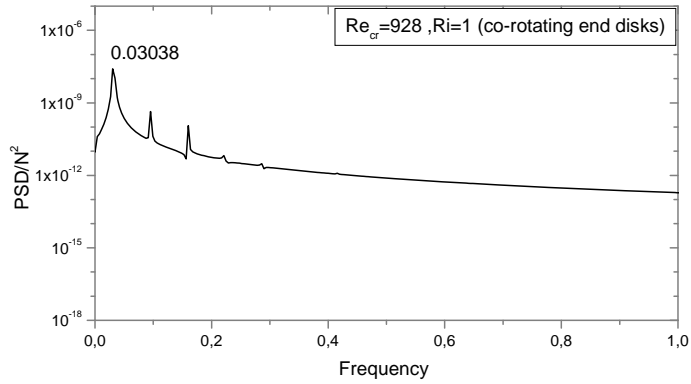


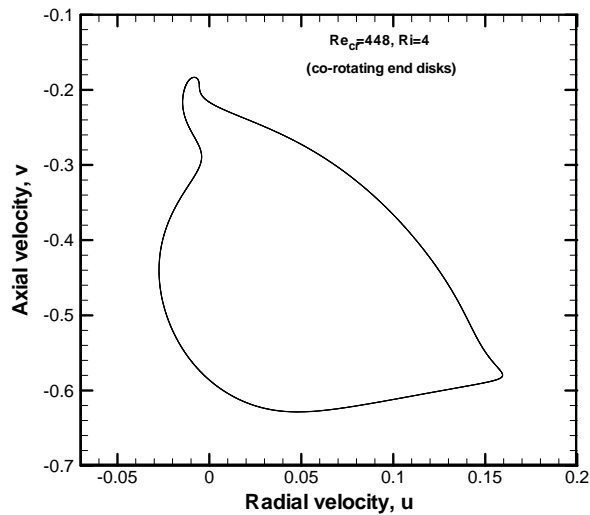
Figure 5: Time histories of dimensionless axial velocity v at monitoring point S5, for $Re=900$, $Re=926$ (steady state) and $Re_{cr}=928$ (the onset of the oscillatory instability).

case as well. We can see that the amplitude of dimensionless temperature oscillations is smaller than that of the dimensionless azimuthal velocity v . The results corresponding to $Ri = 0, 0.5, 1, 2,$ and 4 are represented in the stability diagrams (Fig.12), which highlight the variation of the critical value of the Reynolds number Re_{cr} and the critical frequency F_{cr} , according to the value of the Richardson number, Ri .

It is known that if the Richardson number is much less than unity, buoyancy is unimportant. If it is much greater than unity, buoyancy is dominant (in the sense that there is insufficient kinetic energy to homogenize the fluids). If the Richardson number is of order unity, then the flow is likely to be buoyancy-driven: the energy of the flow derives from the potential energy. We note that the increase of the Richardson number destabilizes the flow. We also note that the flow for counter-rotating disks for the values of the Richardson number $Ri < 1$ is more unstable than the flow in the co-rotating case. For $Ri=1$, the critical Reynolds numbers for both cases of rotation are relatively close. The frequency in the case of $Ri = 0$ (counter-rotating case) is very weak compared to the frequency of co-rotation end disks (Fig.12b and Table 5).

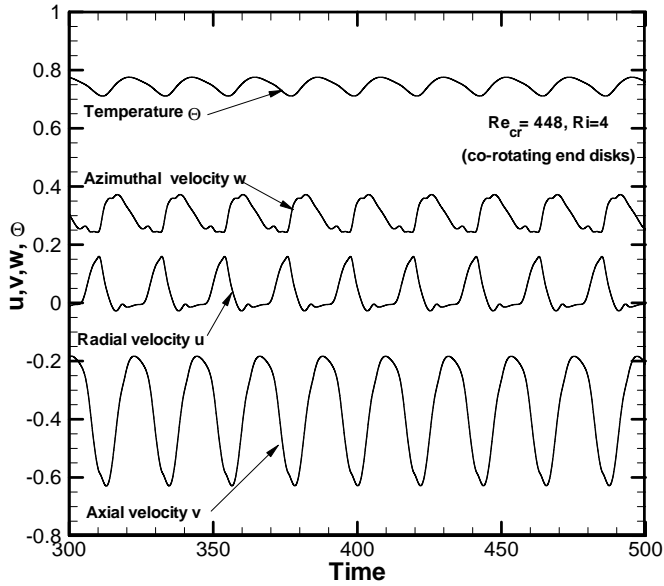


(a)

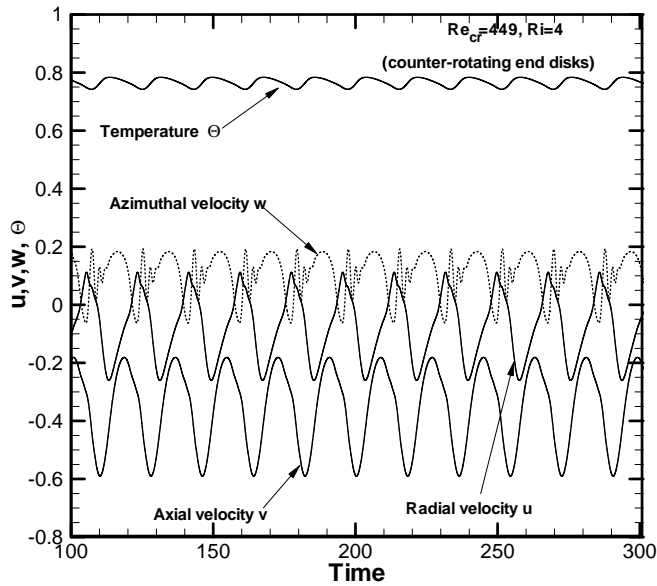


(b)

Figure 6: Co-rotating case: (a) Power spectrum density (PSD) of the dimensionless axial velocity v at point S5, for $Re_{cr}=928$ and $Ri=1$ (b) phase portraits in the plan (u, v) at point S2, for $Re_{cr}=448$ and $Ri=4$.



(a) $Re_{cr}=448$ and $Ri=4$ (co-rotating end disks)



(b) $Re_{cr}=449$ and $Ri=4$ (counter-rotating end disks).

Figure 7: Temporal evolutions of u , v , w , and Θ at point S2

4.2.1 Flow structure in co-rotating case

Figure 8 shows the time history of the axial velocity u over one period of oscillation for $Re_{cr}=928$ and $Ri=1$ (co-rotating case). The period is equal to 32.91 and the corresponding frequency is 0.03038. The streamline patterns in the meridional plane (r - z), the contour plots of isotherms and azimuthal component of the velocity w for various time are shown in Figure 9.

The co-rotating end disks induce a clockwise recirculation region that appears in the upper part of the cylinder and counterclockwise recirculation region in the lower region of the cylinder. It appears that at time $\tau_a=23.61$, the flow presents two cells. These cells dilate and narrow during time ($\tau_a, \tau_b, \tau_c, \tau_d, \tau_e, \tau_f$, and τ_g). Streamlines structures at time $\tau_a=23.61$ are identical to those at time $\tau_g=55.11$, which means that the flow is perfectly periodic. It is also noted at time τ_b and τ_e , that streamlines have opposite structures.

The intermediate layer between the two cells undergoes strong variations in time. The symmetry with respect to mid-height plane at ($z=1$) present in the stable case is no longer a feature of the oscillatory state. At times τ_a, τ_f and τ_g , we observe the appearance of a meridional vortex in the lower corner of the cylinder; but for times τ_c and τ_d the appearance of a meridional vortex in the upper corner of the cylinder. As clearly, shown in contour plots of isotherms (Fig. 9), convective heat transfer dominates the temperature distribution. Plots of the azimuthal velocity w (Fig. 9) indicate that bulk fluid rotates with an intermediate angular velocity with respect to the end disks with boundary layers formed near the rotating disks.

4.2.2 Flow structure in counter-rotating case

Figure 10 shows the time history of the dimensionless streamlines ψ at various times ($\tau_a, \tau_b, \tau_c, \tau_d, \tau_e, \tau_f$, and τ_g) for the case of counter-rotating end disks, and $Re_{cr}=944$ and $Ri=1$ at $S5(0.493, 0.975)$, with the period being equal to 26.06. The corresponding frequency is 0.0337. Streamlines structures shown in Fig.11 present two cells. Cells dilate and narrow during time. At time τ_a , in particular, the cell near the bottom disk forms one counterclockwise recirculation region. This region grows; while the upper clockwise recirculation region becomes smaller. We observe at τ_d and τ_f the appearance of a meridional vortex in the upper corner of the cylinder. Streamlines structures at time τ_a are identical to this at time τ_g which means that the flow is periodic. It is also noted at time $\tau_b=130.04$ and $\tau_f=145.13$, streamlines have opposite structures.

The fluid located in proximity of each disk rotates in the related disk angular direction and shearing flow is created between the top and bottom boundaries, this shearing layer being unstable. The origin of this instability was studied by Nore

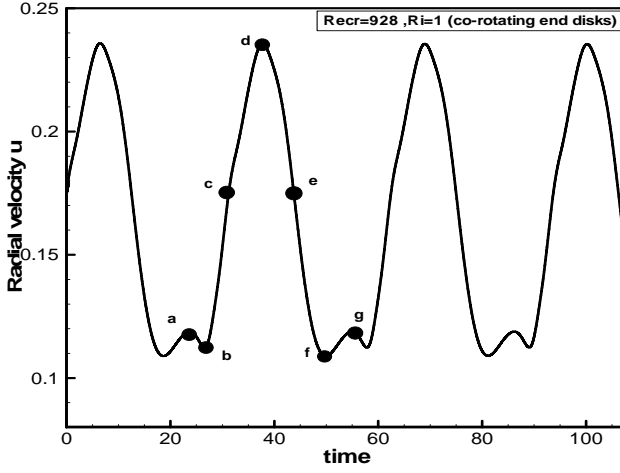


Figure 8: Time history of the dimensionless radial velocity u at point S8, for $Re_{cr}=928$ and $Ri=1$ (co-rotating end disks case). The points a, b, c, d, e, f, and g correspond to times τ_a , τ_b , τ_c , τ_d , τ_e , τ_f , and τ_g , respectively.

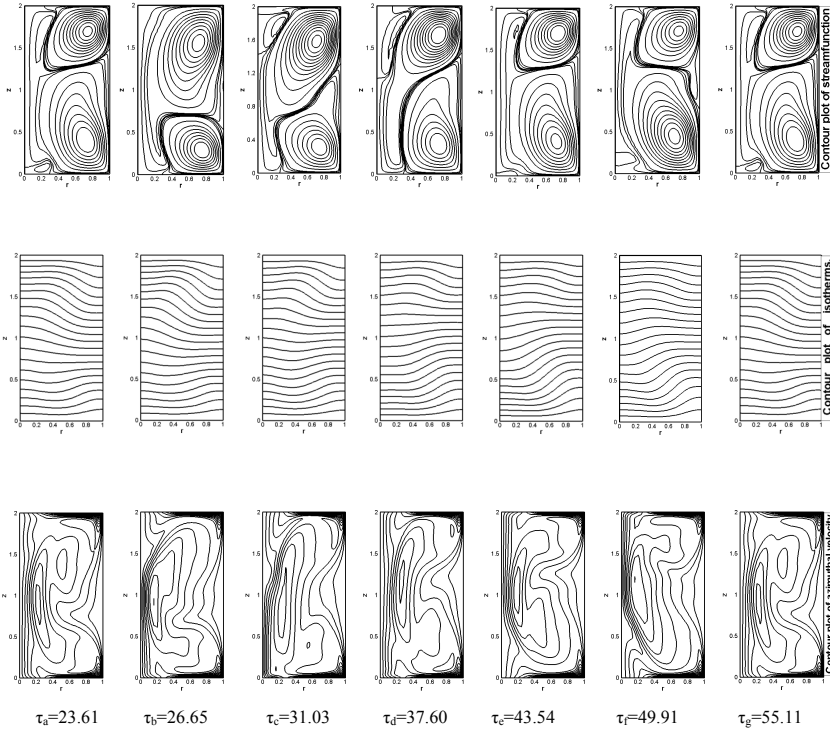


Figure 9: Time history of the dimensionless streamlines ψ , temperature Θ and azimuthal velocity w at various times for $Re_{cr}=928$ and $Ri=1$ (co-rotating end disks case)

et al.(2003) . They studied the exactly counter-rotating case, at a fixed aspect ratio $\gamma=2$, and showed that, when the disk rotation rate is increased, the axisymmetric basic state becomes unstable through a Kelvin-Helmholtz instability of the equatorial azimuthal free shear layer created by the counter-rotation of the top and bottom disks. As made evident by isotherms shown in Fig.11, convective heat transfer dominates the temperature distribution especially in the regions near both rotating disks. Plots of w in Fig.11 indicate that boundary layers are formed on both rotating disks, because of the inhibition of vertical motion by the buoyancy force.

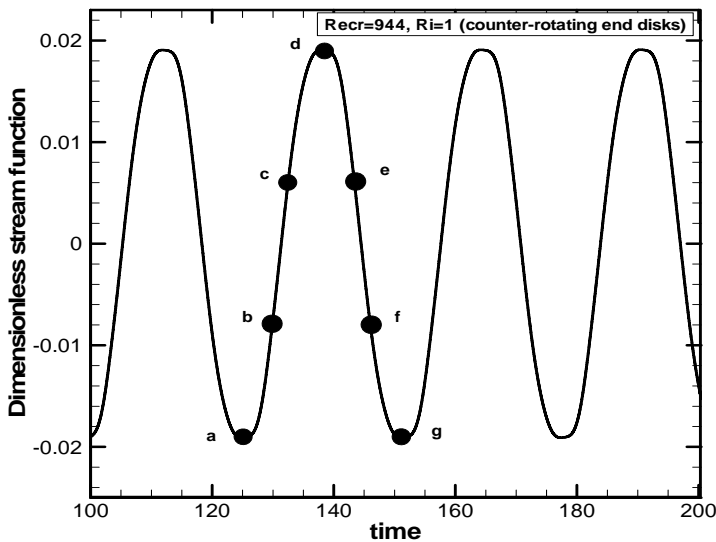


Figure 10: Time history of the dimensionless steam function at point S5, for $Re_{cr}=944$ and $Ri=1$ (counter-rotating end disks case). The points a, b, c, d, e, f, and g correspond to times τ_a , τ_b , τ_c , τ_d , τ_e , τ_f , and τ_g , respectively.

5 Conclusions

Mixed convection in a cylindrical enclosure filled with a liquid metal with co-/counter-rotating end disks and stationary sidewall has been investigated numerically. The finite volume method has been used to solve the transport equations. Numerical simulations have been presented for various values of the Richardson number ($Ri = 0, 0.5, 1, 2, \text{ and } 4$), in order to evaluate the related effect on the critical Reynolds number, Re_{cr} and on the critical frequency of oscillation, F_{cr} . The results show that the flow created by counter-rotating end disks is very different

Table 5: The critical value of the Reynolds number Re_{cr} and their corresponding frequencies F_{cr} for various values of Ri (co- and counter-rotating end disks)

	Co-rotating					Counter-rotating				
	0	0.5	1	2	4	0	0.5	1	2	4
Ri										
Re_{cr}	2645	1475	928	644	448	2284	1278	944	648	449
F_{cr}	0.05720	0.03232	0.03038	0.03975	0.04558	0.01906	0.02456	0.03781	0.04557	0.05688

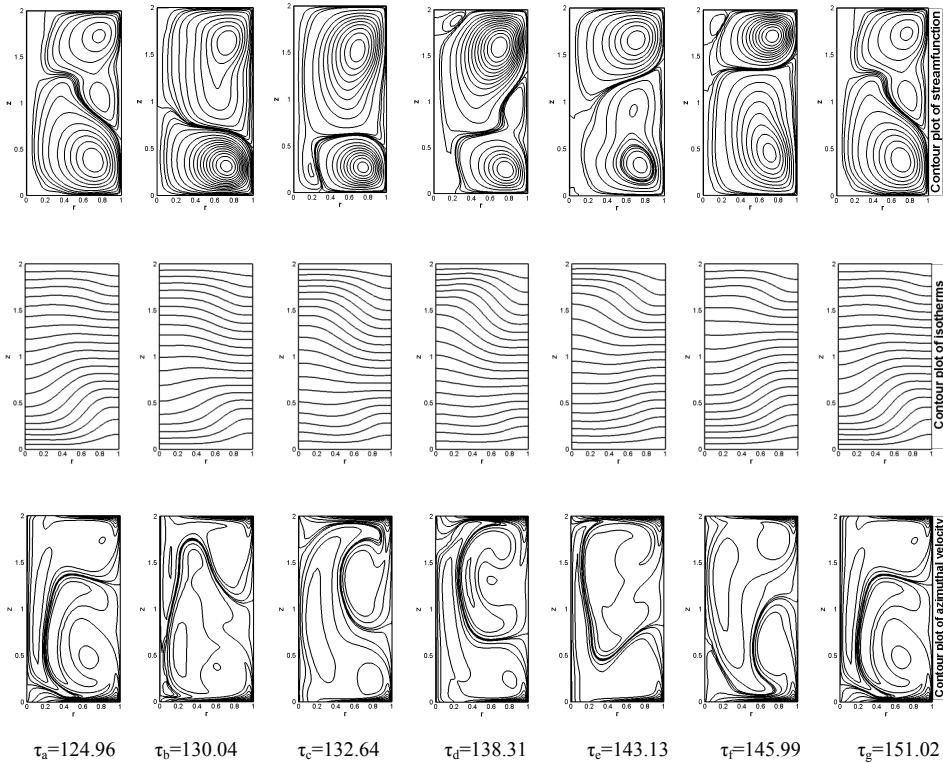


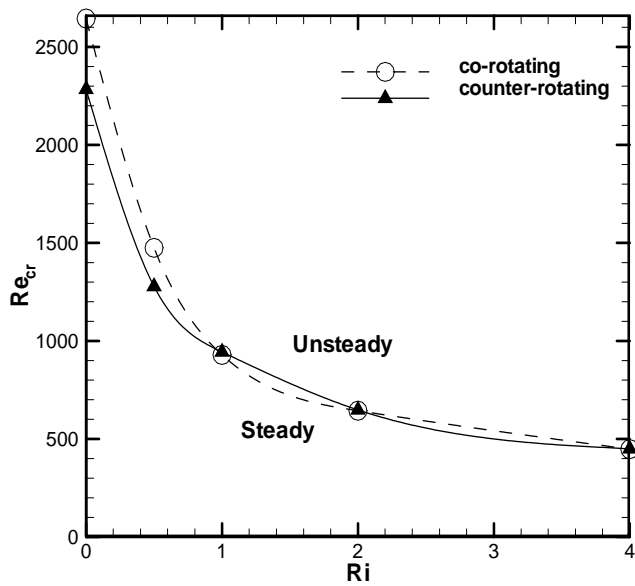
Figure 11: Time history of the dimensionless streamlines ψ , temperature Θ and azimuthal velocity w at various times for $Re_{cr}=944$ and $Ri=1$ (counter-rotating end disks case).

from that in the co-rotating case. For values of the Richardson number ($Ri < 1$), the flow in the counter-rotating case is more unstable than the flow for co-rotating end disks, and causes a remarkable change in the flow and heat transfer structures. For $Ri=1$, the critical Reynolds numbers for both cases of rotation are almost equal. The increase of Richardson number decreases the critical Reynolds number.

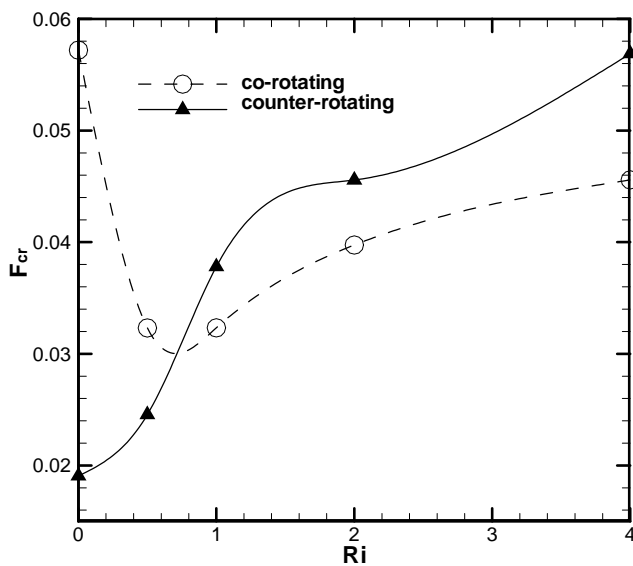
References

Barnes, A. H. (1955): Pumping of Liquid Metals, *International Conference on the Peaceful Uses of Atomic Energy*. vol. 9, pp. 259.

Batchelor, G.K. (1951): Note on a class of solutions of the Navier-Stokes equations representing steady rotationally-symmetric flow. *Quart. Journal of Mechanics*, vol. 1, pp.29–41.



(a) $Re_{cr}-Ri$.



(b) $F_{cr}-Ri$

Figure 12: Stability diagrams.

Bessaih, R.; Marty, Ph.; Kadja, M. (2003): Hydrodynamics and heat transfer in disk driven rotating flow under axial magnetic field. *International Journal of Transport Phenomena*, vol. 5, pp.259–278.

Bordja, L.; Tuckerman, L. S.; Witkowski, L.M.; Navarro, M.C.; Barkley, D.; Bessaih, R. (2010) : Influence of counter-rotating von Kármán flow on cylindrical Rayleigh-Bénard convection. *Physical Review E* 81, 036322.

Brøns, M.; Voigt, L.K. ; Sørensen, J.N. (2001): Topology of vortex breakdown bubbles in cylinder with rotating bottom and free surface. *Journal of Fluid Mechanics*, vol. 428, pp.133–148.

Cui, X. (2008): Cell pattern and stagnation ring of the flow driven by the counter-rotation in a fluid-filled cylinder. *Computers and Fluids*, vol. 37, pp. 135–145.

Dijkstra, D.; Heijst, G.J.F.V. (1983): The flow between two finite rotating disks enclosed by a cylinder. *Journal of Fluid Mechanics*, vol. 128, pp.123–154.

Gelfgat, A.Y.; Bar-Yoseph, P.Z.; Solan, A. (1996a): Steady states and oscillatory instability of swirling flow in cylinder with rotating top and bottom. *Physics of Fluids*, vol. 8, no. 10, pp. 2614–2625.

Gelfgat, A.Y.; Bar-Yoseph, P.Z.; Solan, A. (1996b): Confined swirling flow simulation using spectral Galerkin and finite volume methods. *Proc. ASME Fluids Engineering Division Summer Meeting, FED*, vol. 238, pp.105–112.

Gelfgat, A.Y.; Bar-Yoseph, P.Z.; Solan, A. (1996c): Stability of confined swirling flow with and without vortex breakdown. *Journal of Fluid Mechanics*, vol. 311, no.1, pp. 1–36.

Gelfgat, A.Y.; Bar-Yoseph, P.Z.; Solan, A. (2001): Three-dimensional instability of axisymmetric flow in a rotating lid–cylinder enclosure. *Journal of Fluid Mechanics*, vol. 438, pp.363–377.

Hart, J.E.; Kittelman, S. (1996): Instabilities of the sidewall boundary layer in a differentially driven rotating cylinder. *Physics of Fluids*, vol. 8, pp. 692–696.

Hirano, T.; Guo, Z. ; Kirk, R. G. (2005): Application of CFD Analysis for Rotating Machinery, Part 2: Labyrinth seal analysis. *ASME Journal Of Engineering For Gas Turbines and Power*, vol. 127, pp.820–826.

Iwatsu, R. (2004): Flow pattern and heat transfer of swirling flows in cylindrical container with rotating top and stable temperature gradient. *International Journal of Heat Mass Transfer*, vol. 47, pp. 2755–2767.

Iwatsu, R. (2005): Numerical Study of flows in a cylindrical container with rotating bottom and top flat free surface. *Journal of the Physical Society of Japan*, vol. 7, pp. 333–344.

Jaluria, Y. (2001): Fluid flow phenomena in materials processing-the 2000 Free-

man scholar lecture, Trans. *ASME Journal of Fluids Engineering*, vol. 123, pp. 173–210.

Kim, W.N.; Hyun, J.M.(1997): Convective heat transfer in a cylinder with a rotating lid stable stratification. *International Journal of Heat and Fluid Flow* ,vol. 18, pp.384–388.

Knobloch, E.(1998): Rotating convection: recent developments. *International Journal of Engineering Science* , vol. 36, pp. 1421–1450.

Lopez, J.M. (1998): Characteristics of end wall and sidewall boundary layers in a rotating cylinder with a differentially rotating end wall. *Journal of Fluid Mechanics*, vol. 359, pp. 49–79.

Lopez, J. M. (1995): Unsteady swirling flow in an enclosed cylinder with reflection symmetry. *Physics of Fluids*, vol. 7, pp.2700–2714.

Lopez, J.M.; Perry, A.D. (1992): Axisymmetric vortex breakdown. Part 3:Onset of periodic flow and chaotic advection. *Journal of Fluid Mechanics*, vol. 234, pp.449–471.

Nore, C.; Tartar, M.; Daube, O. ; Tuckerman, LS. (2004): Survey of instability thresholds of flow between exactly counter-rotating disks. *Journal of Fluid Mechanics*, vol. 511, pp. 45-65.

Nore, C.; Tuckerman, LS.; Daube, O.; Xin, S. (2003): The 1:2 mode interaction in exactly counter-rotating von Kármán swirling flow. *Journal of Fluid Mechanics*, vol. 477, pp. 51–88.

Omi, Y.; Iwatsu, R. (2005): Numerical study of swirling flows in a cylindrical container with co-/counter-rotating end disks under stable temperature difference. *International Journal of Heat and Mass Transfer*, vol. 48, pp. 4854–4866.

Patankar, S.V. (1980): *Numerical Heat Transfer and Fluid Flow*. McGraw-Hill, New-York.

Stevens, J.L.; Lopez, J.M.; Cantwell, B.J. (1999): Oscillatory flow states in an enclosed cylinder with a rotating endwall. *Journal of Fluid Mechanics*, vol. 389, pp.101–118.

Stewartson, K. (1953): On the flow between two rotating coaxial disks. *Proc. Camb. Phil. Soc.*, vol. 49, pp.333–341.

Valentine, T.; Jahnke, C.C. (1994): Flows induced in a cylinder with both end walls rotating. *Physics of Fluids*, vol. 6, pp. 2702–2710.

Weltmann , R. N.; Kuhns, P. W. (1952): Effect of shear temperature on viscosity in a rotational viscometer measurement. *Journal of Colloid Science* , vol. 7, pp. 218–226.

Xinjun, C. (2003) :A numerical study of the recirculation zones during spin-up and spin-down for confined rotating flows. *Theoretical Computer of Fluid Dynamics* , vol. 17, pp. 31–49.

Yu, S.C.M.; Ng, B.T.H.; Chan, W.K.; Chua, L.P. (2000): The flow patterns within the impeller passages of a centrifugal blood pump model. *Medical Engineering and Physics*, vol. 22, pp.381–393.